RSC Advances

PAPER

View Article Online
View Journal | View Issue

Cite this: *RSC Adv.*, 2021, **11**, 24694

Fluorescent labeling and characterization of dicarboxylic cellulose nanocrystals prepared by sequential periodate–chlorite oxidation

Xiaozheng Sun, * Yanhua Xue, Jianye Li, Yu Yang, Yu Bai and Yujia Chen

High-performance fluorescent composites are key to the development and improvement of fluorescent molecular probe technology. In this study, cellulose nanocrystals (CNC) with high carboxyl concentrations were prepared *via* sequential periodate–chlorite oxidation. Then, fluorescent cellulose nanocrystals (FCNC) were prepared by attaching 7-amino-4-methylcoumarin (AMC) onto CNC under 4-(4,6-dimethoxy-1,3,5-triazin-2-yl)-4-methylmorpholinium chloride (DMTMM) catalysis. The morphology and fluorescence properties of FCNC were characterized by Fourier transform infrared spectroscopy, X-ray diffraction, transmission electron microscopy, elemental analysis, ultraviolet-visible absorbance, fluorescence spectrophotometry, and fluorescence spectroscopy. The results showed that AMC was grafted onto the CNC surface by an amidation reaction, and the absorption and emission maxima for FCNC were blue-shifted from 350 nm and 445 nm of AMC to 335 nm and 440 nm, respectively. FCNC retained the crystallinity and nano-topography size of the CNC. The fluorescence intensity, quantum yield, and fluorescence lifetime of FCNC showed the same change law; it first increased and then decreased with an increase in the graft density of AMC from 0.201 to 0.453 AMC molecules per nm^2. The FCNC prepared in this study have good optical properties and can be used in the fields of fluorescent molecular probes and biological imaging.

Received 21st June 2021
Accepted 8th July 2021

DOI: 10.1039/d1ra04812k

rsc.li/rsc-advances

Introduction

Fluorescent molecular probes refer to molecules whose fluorescence signals can change correspondingly when a certain substance or a certain physical property of a certain system changes, which can be called the fluorescent molecular probe of a certain substance or certain physical property. Fluorescent probes for ionic and neutral analytes have been widely used in many different fields, such as biology, physiology, pharmacology, and environmental sciences.[1] Compared with the traditional methods of atomic absorption spectrometry,[2] ultraviolet-visible (UV-vis) spectrophotometry, anodic stripping voltammetry[3] and other methods, fluorescent probes have high sensitivity, good selectivity, and convenient use.[4–7] However, the commonly used fluorescent probes exhibit poor hydrophilicity, poor fluorescence stability, weak recombination ability, and susceptibility to environmental influences.[8]

The application of nanocellulose in the field of fluorescent molecular probes is expected to overcome the above-mentioned limitations and improve the performance of fluorescent probes. Nanocellulose is predominantly composed of cellulose, with any external dimension between 1 and 100 nm, and is mainly divided into cellulose nanocrystal (CNC) and cellulose nanofibril (CNF) (ISO/TS 20477). Nanocellulose has a large specific surface area, good hydrophilicity, good biocompatibility, and environmental friendliness.[9,10] Each anhydroglucose unit (AGU) in nanocellulose has three active hydroxyl groups, which can be fluorescently functionalized by electrostatic adsorption and covalent binding.[11] Grafting nanocellulose can maintain the fluorescence intensity of fluorescent molecules and solve the problem of easy self-quenching of high-density fluorescent molecules.[12] Mahmoud *et al.* synthesized two fluorescent cellulose nanocrystals (FCNC) of CNC-fluorescein-5-isothiocyanate and rhodamine isothiocyanate by a three-step method, demonstrating that FCNC can cross the cell and have no cytotoxicity.[13] Grate *et al.* developed two methods to incorporate Alexa Fluor dyes onto CNC, and the spatial localization of solid cellulose deposition could be determined by bioimaging.[14] Leng *et al.* covalently bound fluorescein or rhodamine B to the CNC, and the results showed that the amount of dye grafting and surface functional groups had important effects on fluorescence properties.[15] Abitbol *et al.* studied the effect of charge density on fluorescence labeling, and the results showed that bisulfite hindered fluorescence labeling.[16] Zhang *et al.* synthesized fluorescently labeled nanocellulose with pyrene, and FCNC could quantitatively identify trivalent iron ions.[17] Chen *et al.* combined porphyrin pendants and CNC to produce highly dispersed fluorescent probes by carboxylation, extended esterification,

College of Engineering, Northeast Agricultural University, No. 600 Changjiang Street, HarBin, 150030, China. E-mail: sxz1976@hotmail.com

and dicyclohexyl carbodiimide reactions, with good selectivity and sensitivity to Hg^{2+} in water.[18] There are many methods for binding fluorescent molecules on CNC surfaces in the field of fluorescent probes,[19–21] including amidation reactions,[22] Schiff base reactions,[23,24] and surface ammoniation.[11]

Coumarin is an excellent precursor for the synthesis of fluorescent probes because it a large Stokes' shifts, adjustable photophysical and photochemical properties, high fluorescence quantum yield[25] and good photostability.[26–28] Coumarin is a colorless or buff crystal under visible light, and it can exhibit blue or purple fluorescence under UV light. The absorption and emission spectra of coumarin change when the sites 3 or 4 are substituted by an electron-withdrawing substituent and site 7 is substituted by an electron-pushing substituent.[29–32] Zhang *et al.* used a controlled esterification reaction to carboxylate the surface of CNC and grafted 7-amino-4-methylcoumarin (AMC) to prepare FCNC for the quantitative detection of Cu^{2+}.[12] Huang *et al.* synthesized FCNC by grafting 7-hydrazino-4-methylcoumarin and AMC onto CNC prepared by the sulfuric acid method. They found that the dye was mainly grafted to the surface of the CNC, and a small amount was grafted to the reducing end.[24] Zhao *et al.* synthesized FCNC by grafting coumarin-3-carboxylic acid ethyl ester to CNC prepared by the TEMPO-mediated oxidation method to study the visualization of the composite material interface.[33]

Carboxyl groups are very important functional groups in the functional modification of nanocellulose.[12,22,34,35] CNC are usually prepared by the sulfuric acid method, but the surface of CNC contains bisulfite, which has a hindering effect on fluorescent grafting. The CNC needs to be modified by carboxylation and then grafted with a fluorophore to prepare FCNC.[16] The nanocellulose prepared by TEMPO-mediated oxidation has carboxyl groups on the surface, but the content of carboxyl groups is lower, and the fluorescence intensity is lower after grafting fluorophores. The dicarboxylic CNC prepared by the periodate sequential oxidation method has a higher carboxyl concentration on the surface,[36,37] and a better fluorescence performance is expected by grafting fluorophores. To the best of our knowledge, there is no related research on the fluorescent functional modification of dicarboxylic CNC prepared by sequential periodate–chlorite oxidation.

The objectives of this study are as follows: (1) to develop a method of fluorescence modification of dicarboxylic CNC prepared by sequential periodate–chlorite oxidation; (2) to clarify the grafting mechanism of CNC and AMC and the fluorescence performance of FCNC through Fourier transform infrared spectroscopy (FTIR), X-ray diffraction (XRD), transmission electron microscopy (TEM), UV-vis absorption spectroscopy, fluorescence spectrophotometry, and fluorescence spectroscopy to analyze the morphology and fluorescence characteristics; (3) to investigate the influence of the AMC grafting amount on the fluorescence performance of FCNC and analyze the effect of the density of fluorophores on fluorescence intensity, quantum yield, and fluorescence lifetime.

Materials and methods

Materials

Microcrystalline cellulose (MCC), $NaIO_4$, sodium chlorite ($NaClO_2$), sodium hydroxide (NaOH), and hydrochloric acid (HCl) were purchased from Sinopharm Chemical Reagent Co., Ltd. *N*,*N*-Dimethylformamide (DMF), 4-(4,6-dimethoxy-1,3,5-triazin-2-yl)-4-methylmorpholinium chloride (DMTMM), and AMC were purchased from Aladdin Biochemical Technology Co., Ltd. All materials were used as received without further purification. Deionized water was used for all experiments.

Preparation of dicarboxylic CNC

The dicarboxylic CNC was prepared using a previously reported method.[36] First, 4 g MCC, 5.33 g $NaIO_4$, 15.6 g NaCl, and 266 mL H_2O were placed in a 500 mL beaker, placed on a magnetic stirrer, and kept stirring for 24 h in the dark at room temperature. In sequence, 10 mL of ethylene glycol was added to the beaker, stirring was maintained for 30 min, and the reaction was ended. The resulting product was washed with deionized water, centrifuged (1500*g*, 5 min), and this process was repeated several times until the conductivity of the supernatant after washing and centrifugation was less than 20 μS cm^{-1}. The freeze-dried product was dialdehyde cellulose with a yield of 87%, and the aldehyde content was 3.27 mmol g^{-1}.

Then, 50 mL H_2O, 1 g dialdehyde cellulose, 2.93 g NaCl and $NaClO_2$ and H_2O_2 (with a molarity twice that of the aldehyde content of the dialdehyde cellulose) were added into a 200 mL beaker, and the beaker was placed on a magnetic stirrer for reaction for 24 h. In the reaction process, 0.5 M NaOH solution was added to the reaction solution to stabilize the pH of at 5. At the end of the reaction, anhydrous ethanol was added to the reaction solution at a volume ratio of 1 : 2 and centrifuged after standing for 10 min. The precipitate was washed with 0.5 M HCl, anhydrous ethanol, and deionized water until the conductivity of the supernatant was less than 20 μS cm^{-1} after centrifugation (8500*g*, 5 min). The precipitate was freeze-dried to obtain the dicarboxylic CNC with any external dimension in the nanoscale. The yield of dicarboxylic CNC was 69%, and the carboxyl content was 2.53 mmol g^{-1}.

Synthesis of fluorescent cellulose nanocrystals

First, 0.5 g of dicarboxylic CNC was added to 70 mL of DMF and ultrasonic dispersion was performed for 5 min to ensure that it was evenly dispersed. Then, 0.69 g of DMTMM (the molar concentration of DMTMM was twice the carboxyl molar amount in dicarboxylic CNC) was added and the mixture was placed in a magnetic stirrer for 30 min. Subsequently, AMCs of 1, 3, 5, 7, and 9 times the molar amount of carboxyl groups in the dicarboxylic CNC were added to the reaction solution. The amounts of AMC were 0.22, 0.66, 1.10, 1.54, and 1.98 g, respectively. The reactions were conducted in the dark at room temperature for 24 h. Then, it was washed three times by centrifugation (11 000*g*, 5 min) with DMF, acetone, methanol, and deionized water, respectively. Finally, freeze-drying was performed to

prepare FCNC, which were named FCNC-1, FCNC-3, FCNC-5, FCNC-7, and FCNC-9 according the addition ratio of AMC.

Fourier transform infrared spectroscopy

Fourier transform infrared spectra were recorded on a Nicolet™ iS50 FTIR spectrometer (Thermo Fisher Scientific, China), which has a far-infrared diamond-attenuated total reflectance (ATR) module. In the absorbance mode, in the range of 500–4000 cm^{-1}, the spectrum was recorded in the ATR mode, with 32 scans per spectrum, with a resolution of 4 cm^{-1}. The data were analyzed after subtracting the background data.

X-ray diffraction

XRD measurements were performed on a D8 Advance X-ray diffractometer (Bruker, Germany) using Cu Kα radiation (λ = 0.154 nm) at 40 kV and 30 mA. The scans were performed at room temperature at a speed of 0.7° min^{-1}, and the diffraction data was collected within a 2θ range of 5–40°. The crystallinity index (CI) was determined using the Segal method[38–40] using the following eqn (1):

$$\mathrm{CI} = \frac{I_{200} - I_{\mathrm{am}}}{I_{200}} \times 100\% \quad (1)$$

where I_{200} is the maximum diffraction intensity at 2θ between 22° and 23°, and I_{am} is the minimum diffraction intensity at 2θ between 18° and 19°.

Transmission electron microscope

TEM images were obtained using a JEM-2100F microscope (JEOL, Japan) at an operating voltage of 200 kV. Before the observation, 0.1 wt% of the polymer suspension was spread onto the carbon-coated copper grid to prepare the TEM observation sample, and the observation suspension was dyed with a 2 wt% phosphotungstic acid solution to enhance the image contrast.

Aldehyde and carboxyl content

The aldehyde and carboxyl contents of the CNC were determined using a previously reported method. The hydroxylamine hydrochloride method was used to determine the aldehyde group content of the dialdehyde cellulose. Hydroxylamine hydrochloride can undergo nucleophilic addition and elimination reactions with an aldehyde group to generate oxime and HCl. The generated HCl was titrated with NaOH standard solution, and the aldehyde group content in the dialdehyde cellulose was calculated using the reaction equation. First, a suspension of 0.1 g dialdehyde cellulose and 10 mL deionized water was prepared, 20 mL isopropanol was added, and the mixture was magnetically stirred for 30 min. In sequence, 0.5 M HCl solution was added to adjust the pH value of the suspension to 2–3, and a 0.1 M NaOH standard solution was used to adjust the pH value of the solution to 3.5. Next, 10 mL NH_2OH–HCl solution (10 wt%) was added, the solution was stirred for 30 min, and finally, NaOH (0.5 M) was titrated to the pH of the suspension to 3.5.[41] The amount of NaOH was recorded. The formula for calculating the aldehyde group is as follows:

$$A_{\mathrm{ald}} = \frac{V_{\mathrm{NaOH}} \times N}{W_{\mathrm{c}}} \quad (2)$$

where A_{ald} is the content of the aldehyde group (mmol g^{-1} cellulose); V_{NaOH} is the NaOH (mL) volume; N is the NaOH concentration (0.5 mol L^{-1}); and W_{c} is the weight of the initially suspended dry cellulose (g).

The carboxyl content was determined using the conductometric titration method. First, CNC (0.1 g) was dispersed in 100 mL of 0.1 M NaCl solution and evenly stirred; then, a 0.1 M HCl solution was poured into the solution to adjust the pH value to a value between 2.5 and 3.0, and the volume of the HCl solution used was recorded. Next, the 0.04 M NaOH solution was titrated while continuously stirring. The conductivity change was recorded using an automatic potentiometric titrator (ZD-2, Shanghai LeiCi Magnetic Instrument Co., Ltd.). The carboxyl content of the samples was determined using the conductivity curve. The molar mass concentration of carboxyl groups on the surface of oxidized cellulose was calculated using eqn (3), and three sets of parallel experiments were performed.

$$[\mathrm{COO^-}] = \frac{(C_1 V_1 - C_0 V_0)}{m} \quad (3)$$

where $[\mathrm{COO^-}]$ is the carboxyl content (mmol g^{-1}); C_1 is the equivalent concentration of NaOH standard solution, (M); V_1 is the volume of NaOH standard solution consumed (mL); C_0 is the concentration of HCl solution consumed (M); V_0 is the volume of the added HCl solution (mL); and m is the weight of CNC (g).

Degree of substitution calculation

An elemental analyzer (EA3000, Ovette, Italy) was used to determine the content of N element in the FCNC. Elemental analysis was used to calculate the degree of substitution (DS) of the carboxyl groups on the surface of the FCNC. The traditional measurement of cellulose polymer substitution is the DS per AGU. The nitrogen content can be converted into DS using eqn (4).[24]

$$N\% = \frac{\mathrm{DS} \times 14n}{162 + (\mathrm{DS} \times M)} \quad (4)$$

where N% is the weight percentage of nitrogen in the FCNC sample, DS is the degree of substitution of each AGU in the FCNC, n is the number of nitrogen atoms in the substituent groups, and M is the molecular weight of the substituent group.

Optical characterization

The UV-vis absorption spectra of FCNC were obtained using a high-performance UV-vis spectrometer (Lambda 850, PerkinElmer, USA). The scanning wavelength range was 225–450 nm, and the scanning rate was 1 nm s^{-1}.

A fluorescence spectrophotometer (F-7100, Hitachi, Japan) was used to measure fluorescence spectra. The excitation

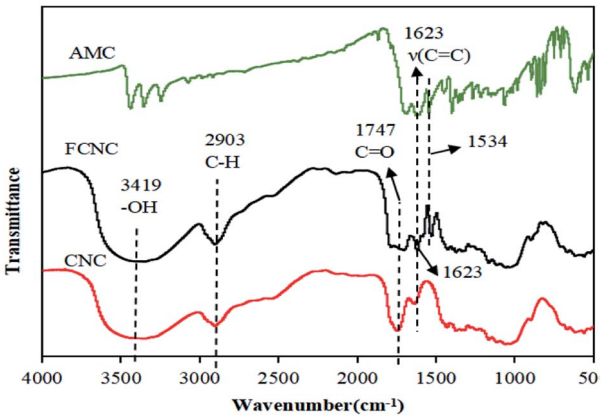

Fig. 1 FTIR spectra of dicarboxylic CNC, AMC, and FCNC.

wavelengths of AMC and FCNC were 350 and 335 nm, respectively.

The fluorescence quantum yield was measured using an absolute quantum yield measuring instrument (C9920-02G, Matuhama, Japan) with an excitation wavelength of 335 nm. The fluorescence lifetime was measured on an FLS920P fluorescence spectrometer equipped with a 450 W xenon lamp (Edinburgh, UK) with an excitation wavelength of 335 nm.

Results and discussion

FTIR analysis

To analyze the changes in the functional groups of the materials before and after grafting, the FTIR spectra of CNC, AMC, and FCNC were obtained, and the results are shown in Fig. 1. The FTIR spectrum of CNC has evident cellulose spectral characteristics: 3419 cm^{-1}, 2903 cm^{-1}, and 1747 cm^{-1} correspond to the tensile vibration of –OH in cellulose, CH, and C=O on the carboxyl group, respectively.[42] In the FTIR spectrum of FCNC, the spectral characteristics of CNC are clearly observed, and two new peaks appeared at 1623 cm^{-1} and 1534 cm^{-1}. The peak at 1623 cm^{-1} corresponds to the C=C tensile vibration of the aromatic ring of AMC on the FCNC surface, and 1534 cm^{-1} corresponds to the N–H bending vibration and C–N tensile

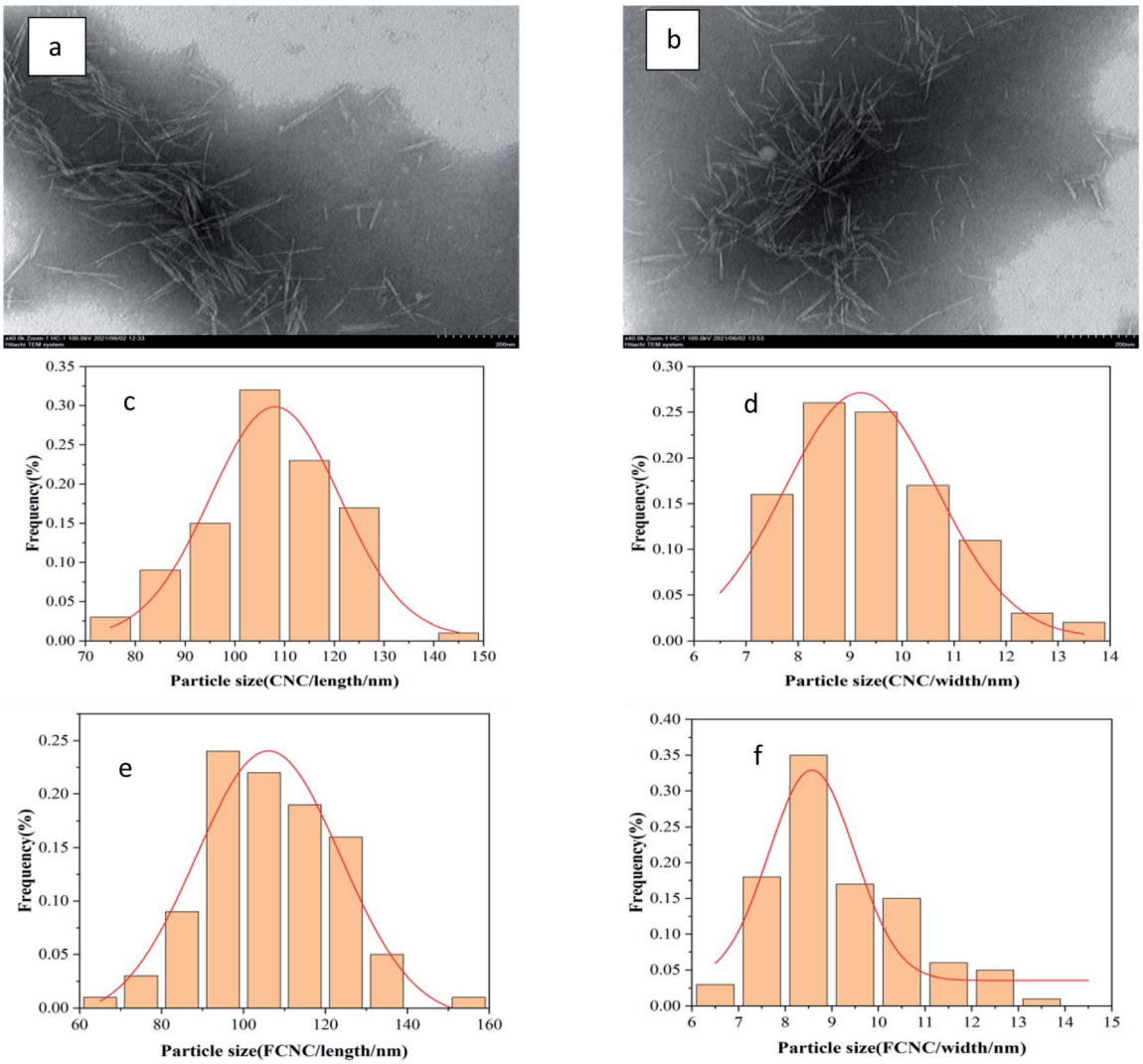

Fig. 2 TEM pictures of (a) dicarboxylic CNC and (b) FCNC; size distribution histogram of (c and d) dicarboxylic CNC, (e and f) FCNC.

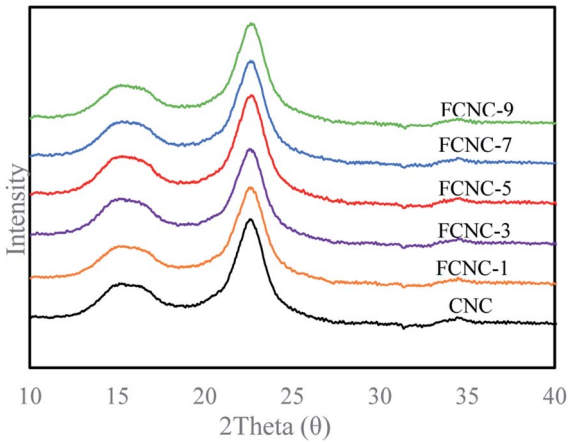

Fig. 3 XRD patterns of FCNC with different AMC grafting concentrations.

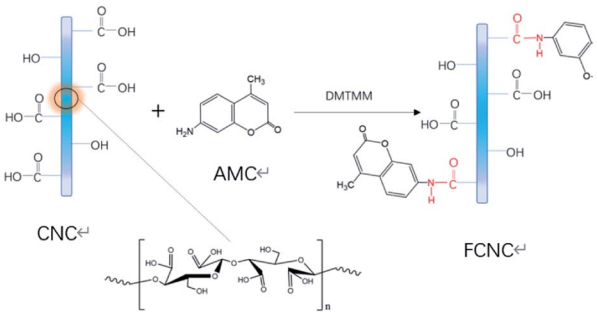

Fig. 4 The reaction mechanism of preparing FCNC by CNC grafting AMC.

vibration of the newly formed amide group. The results indicated that AMC was grafted onto CNC through an amidation reaction.[12]

Morphology analysis of FCNC

To investigate the influence of grafted AMC on the morphology and structure of CNC, the morphology and size of dicarboxylic CNC and FCNC were analyzed by the TEM images and the ImageJ software (particle size statistics). As shown in Fig. 2a and b, the FCNC morphology of the grafted AMC showed no evident change compared to the original CNC. The particle lengths before and after grafting were 106.7 ± 4.0 nm and 105.3 ± 1.9 nm, and the particle diameters were 9.5 ± 0.1 nm and 9.4 ± 0.2 nm, respectively (Fig. 2c–f). This indicates that grafting AMC onto CNC does not change the morphology of the rods and the nanoscale of CNC particles.

Crystallinity analysis

To analyze the effect of grafting AMC on the crystalline form of cellulose, XRD analysis was performed on CNC and FCNC, and the results are shown in Fig. 3. The materials before and after the grafting of AMC had evident diffraction peaks attributed to cellulose I, indicating that FCNC retained the crystal form of the original CNC. The CIs of CNC and FCNC are shown in Table 1, and the statistical difference in the CIs before and after grafting was not significant. This result indicates that the grafting of AMC onto the surface of CNC hardly affected the crystal form of CNC.

Table 1 Crystallinity index of FCNC with different AMC grafting concentrations

Sample	I_{200}	I_{am}	CI (%)
CNC	5413	1058	80.45
FCNC-1	5007	958	80.87
FCNC-3	4912	1084	77.93
FCNC-5	5601	1181	78.91
FCNC-7	5305	1063	79.96
FCNC-9	5188	982	81.07

From the above analysis, the grafting mechanism of CNC and AMC can be inferred, as shown in Fig. 4. The amidation reaction occurred between the carboxyl group on the CNC surface and the amino group of the fluorescent molecule AMC under the catalysis of DMTMM. FCNC were successfully synthesized, and the grafting reaction did not change the morphology or crystallinity of the original CNC. This can be explained that the amidation reaction occurs on the surface of the CNC, and the reaction conditions are relatively mild, so the CNC will not be excessively oxidized to destroy the microstructure of the cellulose, and the morphology and crystallinity are maintained.

Analysis of graft density and graft quantity

The N contents of the FCNC were measured with an element analyzer to calculate the DS of the carboxyl group on the FCNC surface by AMC. The DS, calculated using eqn (4), is shown in Table 2. The nitrogen content increased with the increase in AMC content, and the DS also increased. The DS increased from 0.0131 for FCNC-1 to 0.0297 for FCNC-9. The higher the DS, the more AMC is grafted onto the CNC. As the amidation reaction occurs between the carboxyl group in CNC and the amino group in AMC, the maximum DS of each AGU on the cellulose molecular chain is two. Assuming that every AGU in the sample can be used for the reaction, the DS calculated in Table 2 is based on the total number of AGUs in the CNC; therefore, we define it as DS_{total}.

The grafting reaction usually occurs only at the reducing end and on the crystal surface of the CNC. Based on the CNC length and particle diameter measured above, the number of reaction sites in the FCNC can be estimated. Assuming that the dicarboxylic CNC is a rectangular parallelepiped model with a length of 105.3 nm and a width of 9.4 nm (square section), the microstructure model previously studied was applied.[42] Thus, the values considered were: length of cellobiose of 1.03 nm, lateral interval between cellulose molecular chains of 0.53 nm, and longitudinal interval of 0.61 nm.[42] The number of cellulose molecular chains on the CNC cross section was $(9.4/0.53 + 1) \times (9.4/0.61 + 1) = 307$. The number of AGUs per cellulose chain

Table 2 Element content and substitution degree of FCNC

Sample	FCNC-1	FCNC-3	FCNC-5	FCNC-7	FCNC-9
N (wt%)	0.112	0.134	0.238	0.244	0.248
DS_{total}	0.0131	0.0157	0.0283	0.0292	0.0297

was 105.3/0.515 = 204, and the total number of AGUs contained in a single CNC particle was 62 864. In addition, as there is only one reducing end on each chain, the number of CNC reducing ends was 307 and the surface AGU = (2 × [(9.4/0.53) + (9.4/0.61)]) × 204 = 13 554. Since the reducing end is more reactive than the carboxyl group, we assume that the carboxyl group will undergo an amidation reaction with the amino group of the AMC molecule after all the reducing end reactions are completed. And all the amidated AMC molecules are arranged on the surface of CNC. The number of AMC molecules per CNC particle (N_{AMC}) was estimated with the DS_{total} and the total number of AGUs and the reducing ends (307) in a CNC particle. The concentration of attaching AMC (C_{AMC}, mmol g^{-1} CNC) was calculated with the number of AMC molecules per CNC particle, Avogadro constant (N_A), average particle size of CNC, and the density of cellulose (1.6 g cm^{-3}).[43] The graft density of AMC (D, AMC per nm^2) was estimated by the number of AMC molecules per CNC particle and surface area of CNC particle. They were all shown in Table 3. It can be seen that the amount of AMC molecules grafted on a single CNC particle is 830–1873, which is 0.80–1.80 times of the result (F-Che-CNCs, diameter = 10–50 nm, length = 100–300 nm, 1038 dye molecules per CNC particle) of Ding *et al.*[11] The graft density of AMC is from 0.201 to 0.453 AMC per nm^2, which is 16.56–37.31 times of the result (CNC–RB-4, 0.01214 dye molecules per nm^2) of Leng *et al.*[15] This may be explained that the carboxyl group concentration (2.53 mmol g^{-1}) of the dicarboxylic CNC prepared by sequential periodate–chlorite oxidation in this study is more than that (0.98 mmol g^{-1}) of the previous study of Leng *et al.* and more dye molecules can be grafted onto CNC. In addition, the nitrogen contents of FCNC were calculated using N_{AMC} and CNC microstructure model mentioned above. The correlation coefficient between the calculated nitrogen contents and the measured experimental values is 0.999. The results indicate that the CNC microstructure model used and the calculated N_{AMC} and graft density are reliable.

Table 3 The number (N_{AMC}, AMC per particle), concentration (C_{AMC}, mmol g^{-1}), and density (D, AMC per nm^2) of AMC molecules grafted onto CNC

Sample	DS_{total}	N_{AMC}	C_{AMC}	D
FCNC-1	0.0131	830	0.093	0.201
FCNC-3	0.0157	994	0.111	0.240
FCNC-5	0.0283	1791	0.200	0.433
FCNC-7	0.0292	1842	0.206	0.445
FCNC-9	0.0297	1873	0.209	0.453

Fluorescence properties

Absorption and emission peaks of FCNC. The UV-vis absorption and fluorescence emission spectra of the FCNC aqueous dispersions are shown in Fig. 5. The maximum absorption peak of FCNC is blue-shifted from 350 nm of AMC (measured value, not shown in Fig. 5a) to 335 nm (Fig. 5a). Fig. 5b shows that CNC itself does not emit fluorescence or only weak fluorescence, whereas CNC grafted with AMC shows evident fluorescence characteristics, the fluorescence intensity is clearly enhanced, and the maximum emission peak is blue-shifted from 445 nm of AMC to 440 nm. There are two possible reasons for the blue shift: the effect of unreacted carboxyl groups on the surface of FCNC on AMC. The carboxyl group is an electron-withdrawing group, which can interact with the fused ring with a fluorescence effect in the AMC structure, adsorb electrons similar to large π bonds on the fused ring, and shift the electron cloud on the fused ring. Second, AMC is grafted onto CNC through an amide bond, which causes a blue shift due to the restraint effect of the CNC surface.[12]

As shown in Fig. 5b, the fluorescence intensity of FCNC at 440 nm first increased and then decreased with an increase in the AMC addition ratio. FCNC-5 showed the highest fluorescence intensity. A possible reason for this decrease is that the fluorescent molecules are self-quenched. The higher the density of fluorescent molecules, the more evident is the self-quenching phenomenon. This result is consistent with the results reported

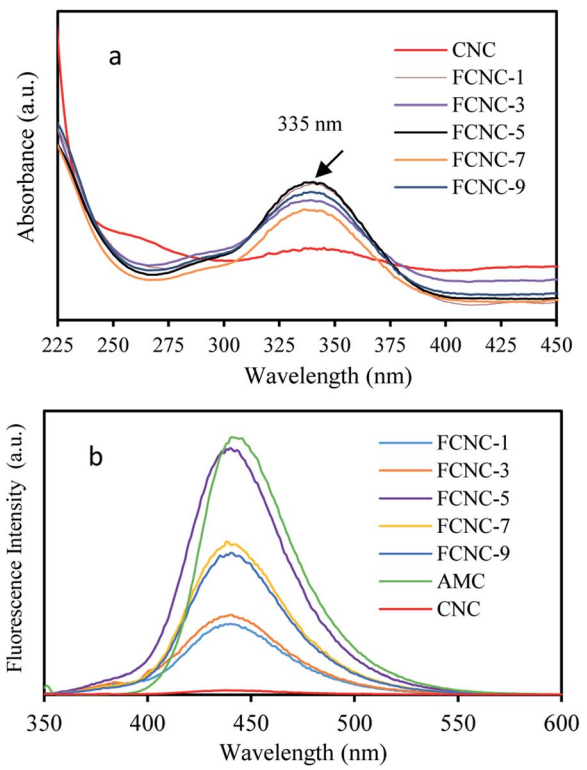

Fig. 5 (a) UV-vis absorption spectra of FCNC aqueous dispersions; (b) fluorescence emission spectra of FCNC aqueous dispersions (excitation wavelength = 335 nm).

Table 4 Comparison of quantum yield and fluorescence lifetime between FCNC and other fluorescence materials

	Quantum yield (%)	Fluorescence lifetime (ns)	Ref.
FCNC-1	9.3	3.45	This study
FCNC-5	15.7	3.69	This study
FCNC-9	9.3	3.46	This study
AMC	30–54	5.0	44 and 45
F-Che-CNC	86	3.9	11
CNC–RB-4	—	2.2	15

by Sîrbu *et al.*[19] This phenomenon can be explained by changes in the density of the fluorophores that affect the fluorescence intensity (Table 3). When the density of AMC molecules grafted onto CNC reached a certain value, the fluorescence intensity was the highest. When the fluorophore density was low, the distance between the fluorophores was larger, and thus the fluorescence intensity was weaker. As the fluorophore density increased, the emitted fluorescence gradually increased. When the density of the AMC molecules reached a certain threshold, the fluorescence intensity reached its maximum. To increase the fluorophore density, the distance between the fluorophores will be closer, and the electron cloud will overlap, such that the fluorescence emission of the fluorophores will affect each other and induce the accumulation of "π–π" and the fluorescence self-quenching effect will appear.[12] In this study, the fluorescence intensity of FCNC-5 was the highest, indicating that maintaining the density of AMC molecules on the surface of CNC at approximately 0.433 AMC per nm^2 helps to maintain a high fluorescence intensity.

Fluorescence lifetime and quantum yield. Fluorescence lifetime and quantum yield are two important indices for characterizing the fluorescence properties of materials. Azuma *et al.* studied the fluorescence quantum yields of 20 coumarin derivatives.[29] The fluorescence quantum yield of coumarin derivatives in different solvents was between 0–83%. The chemical structure of coumarin derivatives is the main factor affecting quantum yield. A comparison of the quantum yield and fluorescence lifetime between FCNC and other fluorescence materials are shown in Table 4. The fluorescence lifetime and quantum yield showed a tendency to increase first and then decrease, and the quantum yield of FCNC-5 (15.7%) and fluorescence lifetime (3.69 ns) were the highest. The fluorescence lifetime of FCNC-5 is 1.68 times that of CNC–RB-4 (CNC and Lissamine rhodamine B ethylenediamine). Although the quantum yield of FCNC-5 is lower than that of AMC and F-Che-CNC, it is higher than that of most coumarin derivatives reported by Azuma *et al.*[29]

The fluorescence stability of FCNC was studied by testing the fluorescence intensity of the fluorescent materials before and after the addition of sodium iodide. The fluorescence intensity of AMC decreased by 43.0% before and after the addition of sodium iodide. In contrast, the fluorescence intensity of FCNC decreased by 21.7% after the addition of sodium iodide. The decreased percentage of FCNC fluorescence intensity was smaller than that of AMC, indicating that the fluorescence stability of the FCNC was improved.

Conclusions

Dicarboxylic CNC with high carboxyl concentrations were prepared by sequential periodate–chlorite oxidation. The FCNC were successfully prepared by grafting the small fluorescent molecules of AMC, and the absorption and emission maxima of the FCNC were 335 and 440 nm, respectively. The analysis results of FTIR and TEM showed that the amide reaction occurred between CNC and AMC, and the rigid structure, rod morphology, crystal form, and CI of the original CNC were not affected by the reaction. The density of the AMC molecules grafted onto the CNC had an important effect on the fluorescence performance of the FCNC. The fluorescence intensity, quantum yield, and fluorescence lifetime of the FCNC first increased and then decreased with an increase in the density of the AMC molecules. The most appropriate density of fluorescent molecules was 0.433 AMC per nm^2, at which the highest fluorescence intensity, quantum yield of 15.7%, and fluorescence lifetime of 3.69 ns were obtained. The FCNC prepared in this study have good optical properties and can be used in the fields of fluorescent molecular probes and biological imaging.

Conflicts of interest

There are no conflicts to declare.

References

1 D. Wu, A. C. Sedgwick, T. Gunnlaugsson, E. U. Akkaya, J. Yoon and T. D. James, *Chem. Soc. Rev.*, 2017, **46**, 7105–7123.
2 Z. Špirić, I. Vučković, T. Stafilov, V. Kušan and M. Frontasyeva, *Arch. Environ. Contam. Toxicol.*, 2013, **65**, 33–46.
3 L. Xiao, H. Xu, S. Zhou, T. Song, H. Wang, S. Li, W. Gan and Q. Yuan, *Electrochim. Acta*, 2014, **143**, 143–151.
4 D. W. Domaille, L. Zeng and C. J. Chang, *J. Am. Chem. Soc.*, 2010, **132**, 1194–1195.
5 T. Xu, J. Huang, M. Fang, M. Sui, Y. Zhu, Y. Shentu, C. Li and W. Zhu, *New J. Chem.*, 2020, **44**, 21167–21175.
6 P. Wang, K. Yao, J. Fu, Y. Chang, B. Li and K. Xu, *Spectrochim. Acta, Part A*, 2019, **211**, 9–17.
7 W. Chen, S. Zhang, G. Dai, Y. Chen, M. Li, X. Zhao, Y. Chen and L. Chen, *Chem.–Eur. J.*, 2019, **25**, 469–473.
8 H. Shaki, K. Gharanjig, S. Rouhani and A. Khosravi, *J. Photochem. Photobiol., A*, 2010, **216**, 44–50.
9 M. Mariano, N. El Kissi and A. Dufresne, *J. Polym. Sci., Part B: Polym. Phys.*, 2014, **52**, 791–806.
10 R. Song, Q. Zhang, Y. Chu, L. Zhang, H. Dai and W. Wu, *Cellulose*, 2019, **26**, 9553–9565.
11 Q. Ding, J. Zeng, B. Wang, W. Gao, K. Chen, Z. Yuan and J. Xu, *Carbohydr. Polym.*, 2017, **175**, 105–112.
12 Y.-J. Zhang, X.-Z. Ma, L. Gan, T. Xia, J. Shen and J. Huang, *Cellulose*, 2018, **25**, 5831–5842.

13 K. A. Mahmoud, J. A. Mena, K. B. Male, S. Hrapovic, A. Kamen and J. H. Luong, *ACS Appl. Mater. Interfaces*, 2010, **2**, 2924–2932.
14 J. W. Grate, K.-F. Mo, Y. Shin, A. Vasdekis, M. G. Warner, R. T. Kelly, G. Orr, D. Hu, K. J. Dehoff, F. J. Brockman and M. J. Wilkins, *Bioconjugate Chem.*, 2015, **26**, 593–601.
15 T. Leng, Z. J. Jakubek, M. Mazloumi, A. C. W. Leung and L. J. Johnston, *Langmuir*, 2017, **33**, 8002–8011.
16 T. Abitbol, A. Palermo, J. M. Moran-Mirabal and E. D. Cranston, *Biomacromolecules*, 2013, **14**, 3278–3284.
17 L. Zhang, Q. Li, J. Zhou and L. Zhang, *Macromol. Chem. Phys.*, 2012, **213**, 1612–1617.
18 J. Chen, Z. Zhou, Z. Chen, W. Yuan and M. Li, *New J. Chem.*, 2017, **41**, 10272–10280.
19 E. Sîrbu, S. Eyley and W. Thielemans, *Can. J. Chem. Eng.*, 2016, **94**, 2186–2194.
20 Y. Xue, Z. Mou and H. Xiao, *Nanoscale*, 2017, **9**, 14758–14781.
21 Z. Zhang, G. Liu, X. Li, S. Zhang, X. Lü and Y. Wang, *ChemElectroChem*, 2020, **85**, 487–502.
22 L. Zhao, W. Li, A. Plog, Y. Xu, G. Buntkowsky, T. Gutmann and K. Zhang, *Phys. Chem. Chem. Phys.*, 2014, **16**, 26322–26329.
23 L. Colombo, L. Zoia, M. B. Violatto, S. Previdi, L. Talamini, L. Sitia, F. Nicotra, M. Orlandi, M. Salmona, C. Recordati, P. Bigini and B. La Ferla, *Biomacromolecules*, 2015, **16**, 2862–2871.
24 J.-L. Huang, C.-J. Li and D. G. Gray, *ACS Sustainable Chem. Eng.*, 2013, **1**, 1160–1164.
25 S. Nad and H. Pal, *J. Phys. Chem. A*, 2001, **105**, 1097–1106.
26 G. He, X. Liu, J. Xu, L. Ji, L. Yang, A. Fan, S. Wang and Q. Wang, *Spectrochim. Acta, Part A*, 2018, **190**, 116–120.
27 J. Yao, W. Dou, W. Qin and W. Liu, *Inorg. Chem. Commun.*, 2009, **12**, 116–118.
28 L. Wang, W. Li, W. Zhi, Y. Huang, J. Han, Y. Wang, Y. Ren and L. Ni, *Sens. Actuators, B*, 2018, **260**, 243–254.
29 K. Azuma, S. Suzuki, S. Uchiyama, T. Kajiro, T. Santa and K. Imai, *Photochem. Photobiol. Sci.*, 2003, **2**, 443–449.
30 J. Griffiths, V. Millar and G. S. Bahra, *Dyes Pigm.*, 1995, **28**, 327–339.
31 X.-B. Wang, J. Zhou, D. Zhang and B. Wang, *Anal. Methods*, 2016, **8**, 6916–6922.
32 J. Li, C. F. Zhang, S. H. Yang, W. C. Yang and G. F. Yang, *Anal. Chem.*, 2014, **86**, 3037–3042.
33 Y. Zhao, W. Dang, Q. Ma and Y. Zhu, *Cellulose*, 2019, **26**, 4345–4355.
34 A. Kumar, I. A. I. Matari, H. Choi, A. Kim, Y. J. Suk, J. Y. Kim and S. S. Han, *Mater. Sci. Eng., C*, 2019, **104**, 109983.
35 A. Kumar, I. A. I. Matari and S. S. Han, *Biofabrication*, 2020, **12**, 025029.
36 X. Sun, Q. He and Y. Yang, *J. Renewable Mater.*, 2020, **8**, 447–460.
37 G. Patterson and Y. L. Hsieh, *Nanoscale Adv.*, 2020, **2**, 5623–5634.
38 L. Segal, J. Creely, A. E. J. Martin and C. Conrad, *Text. Res. J.*, 1959, **29**, 786–794.
39 A. D. French, *Cellulose*, 2014, **21**, 885–896.
40 A. D. French and M. Santiago Cintrón, *Cellulose*, 2013, **20**, 583–588.
41 U.-J. Kim, M. Wada and S. Kuga, *Carbohydr. Polym.*, 2004, **56**, 7–10.
42 L. Song, X. Pei, R. Li, H. Chen and X. Sun, *J. Renewable Mater.*, 2020, **8**, 1269–1282.
43 A. B. Stefaniak, M. S. Seehra, N. R. Fix and S. S. Leonard, *Inhalation Toxicol.*, 2014, **26**, 733–749.
44 C. A. M. Seidel, A. Schulz and M. H. M. Sauer, *J. Phys. Chem. C*, 1996, **100**, 5541–5553.
45 X. Song, J. Chen, X. Zhang and G. Xu, *Chin. Sci. Bull.*, 1991, **36**, 1000–1003.